RSC Advances

ROYAL SOCIETY OF CHEMISTRY

www.rsc.org/advances

Cyclic Tetra [(Indolyl)-tetramethyl]-diethane-1,2-diamine (CTet) Impregnated Hydrous Zirconium Oxide as a Novel Hybrid Material for Enhanced Removal of Fluoride from Water Samples.

Nafisur Rahman* , Uzma Haseen[a] and Mohammad Fazeel Khan[b]

* Corresponding author:
Department of Chemistry, Aligarh Muslim University, and
Aligarh, India 202 002 Tel.:+91-9412501208,
Email id: nafisurrahman05@gmail.com

[a]Department of Chemistry,
Aligarh Muslim University, Aligarh-202002 (U.P.), India.
Email id: uzma.haseen@gmail.com

[b]Department of Chemistry, Aligarh Muslim University,Aligarh-202002 (UP),India
Email id: fazeel.alig@gmail.com

Abstract:

A hybrid material was prepared by incorporating cyclic tetra [(indolyl)-tetra methyl]-diethane-1,2-diamine (CTet) into hydrous zirconium oxide (HZO) via thorough mixing of previously prepared CTet in methanol and stirred for 7 h at 27℃. CTet-HZO was characterized by FT-IR, ^{13}C NMR, XRD, TGA-DTA, SEM coupled with EDX and TEM. The adsorption capacity of fluoride as a function of pH, sorbent dose, contact time, initial concentration of fluoride ions and temperature was examined in batch mode. Maximum fluoride adsorption (188.68 mgg^{-1}) occurred in the pH range 3.5-4.5. The outstanding fluoride sorption property might be ascribed due to the presence of indole-NH groups. The Langmuir, Freundlich and Temkin isotherms were applied to fit the sorption equilibrium data. Based on R^2 and average percentage error (APE), the best isotherm model fits follow the order: Freundlich> Temkin > Langmuir. The pseudo-second order kinetic model well fitted the sorption kinetic data which supported the chemisorption as the mechanism of interaction between sorbent and F^-. The hybrid material could be reused upto four sorption-desorption cycles with no significant decrease in F^- sorption capacity. The material has been applied successfully for the defluoridation of groundwater and river water.

Keywords: cyclic tetra [(indolyl)-tetramethyl]-diethane-1, 2-diamine (CTet), hydrous zirconium oxide, adsorption, fluoride, enhanced removal.

TOC/ Abstract Graphics:

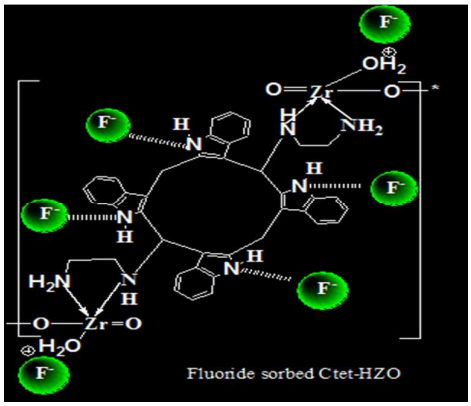

1. Introduction:

Elemental fluorine is the most electronegative [1] and is widely dispersed as fluoride in the environment which is about 0.06-0.09 % of the earth's crust.[2] The release of fluoride to groundwater is dependent on the chemical and physical processes occurring between the groundwater and its geological environment.[3,4] Fluoride enters human body mainly through drinking water and food. The dental health benefits are obtained when the concentration of fluoride in drinking water is 0.8-1.0 mgL^{-1}.[5, 6] U.S. Environmental protection agency has recommended 4.0 mgL^{-1} as maximum contaminant level for fluoride in drinking water,[7] while WHO has set 1.5 mgL^{-1} as a permissible limit.[8] However, if the fluoride concentration in drinking water exceeds the permissible limit, it can pose a health threat to millions of people around the world. The excessive intake of fluoride may cause dental [9] and skeleton disorder.[10] The risk of fluorosis associated with such water for human consumption is a problem faced by many countries of Asia, Africa, America and Europe where the fluoride concentration ranged from 0.01 to 3 mgL^{-1} in fresh water and 1-3.5 mgL^{-1} in groundwater.[11,12]

In recent years, several defluoridation processes such as precipitation,[13] reverse osmosis,[14] nanofiltaration,[15] electrocoagulation,[16] electrodialysis,[17] adsorption and other methods have been studied for the removal of fluoride from aqueous systems. Among various methods, the adsorption process is widely used and offers satisfactory results. The adsorption process seems to be more attractive for removal of fluoride in terms of cost, easy availability of adsorbent, simplicity of design and operation.[18] Many inorganic adsorbents such as Al-Fe (hydr) oxide,[19] Mg-doped nanoferrihydrite,[20] titanium hydroxide derived adsorbent,[21]alginate entrapped nanostructure Al(III)-Ce(IV) mixed oxide [22] and bismuth oxide [23] have been tested for removal of fluoride from water. Hydrous zirconium oxide exhibited high affinity towards fluoride through Lewis acid-base interaction and used as an effective sorbent for defluoridation. In addition, inorganic-organic hybrid materials have also the ability to remove

fluoride from aqueous solution at solid-liquid interface. Adsorption potential of a combination of polymeric anion exchange resin and iron oxide with a goethite (α-FeOOH) structure has been assessed for fluoride removal from water [24]. Swain et al [25] have synthesised zirconium (IV) ethylenediamine hybrid sorbent which showed maximum fluoride removal efficiency at pH 7. Recently, a porous polystyrene encapsulated zirconium phosphate nanocomposite was reported for fluoride ion retention and its adsorption capacity was found to be 6.65 mg/g at pH 3.[26]

The main objective of present study is to develop a hybrid material by impregnating cyclic tetra [(indolyl)-tetra methyl]-diethane 1, 2-diamine(CTet), an indole derivative, into hydrous zirconium oxide (HZO) and to evaluate its properties for efficient fluoride removal from water samples. Previously, indole-3-carbinol cyclic tetramer derivative was used as a promising anticancer agent with antiproliferative activity in breast cancer cells.[27]Single-walled carbon nanotubes have been functionalized for delivery of indole-3-carbinol cyclic tetrameric derivative to breast cancer cell lines in an efficient way.[28] Moreover, polypyrrole and indole derivatives have been identified as potential ligand and ion sensing scaffold.[29] Recent studies have suggested that these materials have high potential for binding with fluoride through indole NH----F^- interaction.[30] Functionalization of hydrous zirconium oxide with CTet would exhibit enhanced fluoride retention owing to the increased number of indole –NH groups in the hybrid material. To the best of our knowledge, no literature is available concerning the immobilization of CTet on any hydrous metal oxide for defluoridation.

2. Experimental methods

2.1. Reagents.

Sodium fluoride (Merck, India) was used for the preparation of stock solution of fluoride (1000 mgL^{-1}) by dissolving an appropriate amount in distilled water and stored in polyethylene bottle. 2, 3-Benzopyrrole (indole) was purchased from Himedia, (Mumbai,

India). Formaldehyde, ethylenediamine, ammonia, acetic acid, and zirconium oxychloride were obtained from Merck (Mumbai, India). Water used in all experiments was doubly distilled.

2.2. Preparation of cyclic tetra [(indolyl)-tetra methyl]-diethane 1,2-diamine (CTet)

The synthesis of 2, 3,-dimer of Mannich base, (*N1*-[(1H-Indol-2-yl)-(1H-indol-3-yl)-methyl]-ethane-1,2-diamine), was carried out according to the procedure reported in literature. [31] To a solution containing 2,3-dimer of Mannich base (10.0 mmol) and formaldehyde (37 %, 14.6 mmol) in methanol, 4.0 mL of acetic acid (99.8%) was added and the mixture was refluxed in dark for 2 h. After cooling, dark wine red solution was obtained and kept, further, for 24 h in mother liquor for complete polymerization, (Scheme S1, SI). The resulting product is CTet (Scheme1).

2.3. Functionalization of Hydrous Zirconium oxide with CTet

Aqueous solution of zirconium oxychloride (0.1 M) was warmed at 70℃ and hydrolized by drop wise addition of 0.1 M NaOH solution following the procedure reported in literature.[32, 33] The white gel formed was aged with supernatant for 2 days at room temperature. The obtained CTet solution was mixed with the (HZO) for 7 h with continuous stirring for complete impregnation of organic moieties. Finally the reaction mixture was filtered and precipitate was washed several times with water, and dried at 50℃ . The final product (CTet-HZO) was broken in to small granules on treatment with distilled water. The chemical and elemental analysis of CTet-HZO shows the following composition: Zr = 19.18 %, C = 50.50 %, H =5.09 % and N = 11.78.The functionalization of hydrous zirconium oxide with CTet is shown in Scheme 2.

2.4. Characterization of CTet-HZO.

The Fourier transform infrared (FT-IR) spectra of HZO and CTet-HZO were recorded with Perkin Elmer FTIR spectrometer (Interspec 2020, Spectrolab, UK) using KBr pellet method. Far infrared spectra (FIR) were obtained by using a Perkin Elmer FT-IR/FIR Fourier spectrometer (wavenumber range 400 to 30 cm^{-1}).The powder X-ray diffraction (XRD) analysis was done by the Panalytical's X'Pert Pro X-ray diffractometer. The radiation used is Cu Kα whereas nickel metal is used as beta filter. Scanning electron micrographs (SEM) coupled with EDX spectra of the material were taken by scanning electron microscope (JEOL JSM-6100 LV Tokyo, Japan), for surface morphology. Transmission electron micrographs (TEM) were also recorded using transmission electron microscope (JEOL JSM 2100, Japan). ^{13}C NMR spectrum was recorded using Bruker Avance III spectrometer with solid state attachment CP-MAS (500 MHz). A Shimadzu TGA/DTA simultaneous measuring instrument, DTG-60/60H (Kyoto, Japan) was used for thermogravemetric analysis (TGA), differential thermal analysis (DTA) and differential scanning calorimetry (DSC) at a heating rate of 10℃ /min under nitrogen atmosphere. The concentration of fluoride was measured using expandable ion analyzer with the fluoride ion selective electrode (ELICO- LI126, India).

2.5. Batch adsorption Experiments:

Batch experiments were conducted by using the traditional bottle-point method to determine the fluoride adsorption equilibrium and kinetic properties of CTet-HZO. A 50 mL fluoride solution at a desired concentration level (20-900 mg/L) was transferred to 100 mL polyethylene bottles. The pH of each solution was fixed at 3.5, except the influence of pH experiment. CTet-HZO (0.15g) was added to the solution and agitated in an incubator shaker at 200 rpm. Effect of pH on the fluoride adsorption onto CTet-HZO and HZO was studied

separately in the pH range 0.5-10 at an initial fluoride concentration of 20 mgL^{-1}, maintaining the other parameters of the experiment constant.

Adsorption kinetics and thermodynamic studies were carried out by adding 0.15 g of CTet-HZO into a series of polyethylene bottles containing 50 mL solution with a fixed initial fluoride ion concentration (20 mgL^{-1}) at pH 3.5 and different temperatures 308, 318 and 328 (± 1) K. At a preselected time intervals, the samples were extracted from the polyethylene bottles. After each experiment, CTet-HZO particles were separated immediately by filtration through 0.45 µm membrane filter. Fluoride concentration of each filtrate was determined by ion analyzer using fluoride ion selective electrode. The amount of fluoride adsorbed at equilibrium (q_e, mg g^{-1}) was calculated by following equation:

$$q_e = \left(\frac{C_o - C_e}{m}\right) V \qquad (1)$$

where C_0 and C_e are initial and equilibrium concentrations of fluoride (mgL^{-1}), respectively, m is the mass of CTet-HZO (g) and V is volume of the solution (L).

2.7. Column experiments:

Fixed bed column experiments were carried out by packing 0.83 g of CTet-HZO or HZO into two separate glass columns (1.0 cm in diameter and 25.0 cm length). The synthetic feeding solution was prepared by adding fluoride (5 mg L^{-1}) to the tap water (free from fluoride) and was allowed to percolate through the column at a constant flow rate (2.5 mL/min). To examine the feasibility of CTet-HZO and HZO for practical application, the groundwater and acidic industrial wastewater, collected from Agra and Aligarh districts of Uttar Pradesh, India, respectively, were also employed as the feeding solution. Percolation of sample solution was stopped when the concentration of fluoride in the effluent exceeded the permissible limit of 1.5 mg L^{-1}.

3. Results and Discussion:

3.1. Physicochemical Characterization of CTet-HZO adsorbent

FTIR spectrum of HZO (Figure 1a) showed absorption bands at wave numbers 3355, 1622, 1556, 1447, 1412, 1130, 1080, 651 and 473 cm^{-1}. The bands around 3355 and 1622 cm^{-1} are assigned to stretching and bending modes of coordinated water and O-H, respectively. The peak at 1130 cm^{-1} is assigned to the bending vibration of hydroxyl group of Zr-OH. [34] The bands at 651 are assigned to Zr-O linkage, respectively.[35] FT-IR spectrum (Figure 1b) shows absorption bands at 3410 and 1619 cm^{-1} are due to-N-H stretching and bending vibrations. In these regions, the coordinated water molecules also absorb radiation. The band appearing at 2928 cm^{-1} may be assigned to –C-H stretching vibration of methylene group. The presence of C-N stretching absorption of primary aliphatic amine is confirmed by the band at 1087 cm^{-1}. The band peaking at 1458 cm^{-1}, 1412 and 1344 cm^{-1} may be assigned to –C=C in-plane vibration and C=N stretching vibration of indole.[35] Another peak at 744 cm^{-1} is attributed to ortho-disubstituted benzene. [35] Far IR spectra of CTet-HZO and fluoride adsorbed CTet-HZO are presented in Supporting Information (Figure S1,a-b, SI). CTet-HZO in Cl^- form shows absorption bands at 229.33, 180, 155 &104 cm^{-1}; while fluoride sorbed CTet-HZO shows strong bands at 290, 200, 157, 120, 96 and 48 cm^{-1}. The peak at 104 disappeared suggested the sorption of fluoride on CTet-HZO [36] The two strong absorption bands (both spectra) at 324 cm^{-1} and 229 cm^{-1} are due to the N-Zr-N in plane bending. [34]

The X-ray diffraction patterns of the adsorbent before and after fluoride adsorption are shown in Figure 2. XRD study reveals the amorphous nature of CTet-HZO with some change after the adsorption of fluoride ions. The fluoride ion sorbed material showed peak at 29.61 with d-spacing of 1.49 *A*°. SEM images of HZO, CTet-HZO and fluoride sorbed CTet-HZO are shown in Figure 3(a-c). HZO (Figure 3a) showed the agglomerated surface morphology with irregular shape and porous nature. SEM image of CTet-HZO showed some changes in the

surface morphology owing to incorporation of CTet. The surface of the adsorbent before and after fluoride adsorption seems to be more or less similar. However, EDX spectrum (Figure S2, SI) confirmed the presence of fluoride on the adsorbent surface. TEM image of CTet-HZO is shown in Figure 4 .The particles of CTet-HZO have irregular shape and very broad in size distribution ranging from 60.5 nm-189 nm. Figure 5 shows ^{13}C NMR spectrum of CTet-HZO. The chemical shifts observed at 137.19 ppm, 128.70 ppm,120.30 ppm and 110.53 ppm indicated the presence of C=C, aromatic carbon, -C- on ortho position of benzene ring, and aryl carbon, respectively. The chemical shifts at 64.03 ppm and 55.14 ppm indicated the presence of C-N linkage and –CH aliphatic, respectively. The peaks at 32.87 & 30.62 ppm confirmed the $–CH_2$ group. Tertiary alkyl carbon appears at 15.48 ppm while the shift at 21.04 ppm suggested the presence of C at 3 position of pyrrole.

The results of thermal analysis of HZO and CTet-HZO are presented in Figure 6 (a&b). TGA curve of HZO indicated the weight loss in the temperature range of 30 to 350 ^{o} C and was attributed to dehydration of the interstitial water.[37,38] DTA curve showed one endothermic peak at 75 ^{o}C ,indicating the loss of water molecules. In case of CTet-HZO, the weight loss occurred in two steps; 16.94% and 15.51 % from 40℃ -190℃ and $> 190 - 440$ ℃ , respectively, corresponding to physically adsorbed water and dehydroxylation from OH groups. The DTA curve showed an endothermic peak at 72.41 ℃ . However, on increasing the temperature above 440 ℃ , sharp deflections in the TGA curve was observed which is attributed to the decomposition of organic molecule present in the matrix. The DTA curve showed an exothermic peak at 450 ℃ which also confirmed the decomposition of organic molecule and two step weight loss. DSC curve of CTet-HZO (Figure S3, SI) showed an endothermic peak at 96 ℃ which also confirmed the loss of water molecules.

Adsorption of Fluoride on CTet-HZO

3.1.1. Effect of pH, Contact time and Sorption mechanism

The pH of the aqueous system is one of the most important parameters which directly affect the fluoride adsorption process. Figure 7 shows the effect of pH on the fluoride uptake by CTet-HZO at 308±1K. Results indicated that the maximum adsorption of fluoride occurred in the pH range 3.5-4.5. Fluoride has different species in water,[39] including HF, HF_2^- and F^-.The pKa of hydrofluoric acid is 3.18 and therefore, free fluoride ions are available for ligand exchange/ hydrogen bonding at pH>3.18. At pH 3.5, OH groups attached to Zr (IV) are protonated and thus promote the adsorption of F^- ions. On the other hand, at pH<3.5 uptake of fluoride decreased that may be due to the non-availability of free fluoride ions. At higher pH, the decrease in uptake of fluoride ions may be attributed to the presence of OH^- which caused the deprotonation of the OH_2^+ groups in the structure. Under this condition the fluoride ions are repelled through electrostatic repulsion. This trend is similar to fluoride ion retention on polystyrene anion exchanger supported hydrous zirconium oxide nanoparticle. [40] The effect of pH on the uptake of fluoride by HZO was also studied. The maximum adsorption was observed in the pH range 6-7 (Figure S4, SI).The adsorption of fluoride on CTet-HZO (pH 3.5) and HZO (pH6.5) was studied as a function of contact time. Results (Figures S5, S6, SI) indicated that the adsorption equilibrium was attained in 40 min with CTet-HZO whereas 90 min are needed for HZO.

The effect of solution pH on the stability of CTet-HZO was studied. It was observed that the leaching of Zr(IV) occurred at pH <2.6. At pH 2.8, 0.08% Zr(IV) and 0.11% cyclic diamine of CTet-HZO were leached into the surrounding solution when immersed for three days. However, Zr(IV) and cyclic diamine were not detected in the residual solution when pH was above 3.0, suggesting the stability of the CTet-HZO.

Recent ^{1}H-NMR study [30] suggested that indole NHs interacts with fluoride ion through hydrogen bonding. In our study, CTet-HZO possess four indole-NH groups and providing

four binding sites for fluoride ion which is indicative of enhanced fluoride sorption. The adsorption mechanism is shown in scheme 3.

The effect of the increased adsorbent dosage on the percent removal of fluoride was studied by varying the amount of adsorbent dose from 0.05-0.4 g/50mL. The experiment was carried out using initial fluoride ion concentration of 20 mgL^{-1} at pH 3.5, keeping the contact time of 40 min. Results (Figure S7, SI) revealed that the removal efficiency increased with increase in adsorbent dose and the value reaches a maximum (98.67%) corresponding to a feeding dose of 0.15 g. The observed results could be attributed to increase in surface area with increase in adsorbent dose and hence more adsorption sites are available for fluoride adsorption.

It is well known that the common ions such as Cl^-, NO_3^-, SO_4^{2-}, HCO_3^-, CO_3^{2-}, and PO_4^{3-} are ubiquitous in drinking water and wastewater. These ions can compete for adsorption sites and decrease the removal efficiency of the adsorbent. Fluoride adsorption in presence of potential co-existing ions was studied to elucidate the outstanding selectivity of CTet-HZO. Hence the tests were conducted in the presence of co-existing ions in the broad range of concentrations (1-1000 mgL^{-1}) and results are shown in Figure 8. It is evident from the figure that the removal efficiency of F^- is not affected in presence of these co-existing ions. However, presence of arsenate ion decreases the removal efficiency of fluoride ion.

3.2. Sorption Studies and Modelling

For optimization of the process for fluoride removal, it is important to understand fluoride ion distribution between two phases via analyzing the adsorption equilibrium data. In this study, the equilibrium data obtained for initial fluoride ion concentration variation from 100 to700 mgL^{-1} at pH 3.5 were investigated by Langmuir, Freundlich and Temkin adsorption isotherm models. The significance of isotherm equations has been highlighted in a number of research articles. [41]

The linear form of Langmuir adsorption isotherm [42] equation is expressed as:

$$\frac{1}{q_e} = \left(\frac{1}{K_L\ q_m}\right)\frac{1}{C_e} + \frac{1}{q_m} \qquad (2)$$

where q_e is the amount of solute adsorbed per unit weight of adsorbent (mg/g) and C_e is the equilibrium concentration in solution (mg/L). The values of q_m and K_L, (Langmuir isotherm constant) relate to the monolayer adsorption capacity (mg/g) and energy of adsorption process. The plots between $1/q_e$ and $1/C_e$ at different initial concentrations and temperatures generate straight line (Figure 9a). The isotherm parameters were calculated and represented in Table. 1. The maximum adsorption capacity of CTet-HZO was found to be 188.6 mg/g.

The performance of CTet-HZO for fluoride adsorption was compared with some previously prepared adsorbents and hydrous zirconium oxide (HZO) prepared in this study (Table 2). The comparative data indicated the superiority of our material over others, mainly in terms of adsorption capacity and contact time. For example, modified carbon nanotubes (CNTs) [46] and graphene (GO) [51] show sorption capacity of 15 mg/g and 48.31 mg/g, respectively. These materials are costly and also a large-scale application of CNTs and GO is limited because of its comparatively higher operational cost. In this reference, CTet-HZO was found to be cheap, efficient and also highly selective adsorbent with high sorption capacity (188.68 mg/g) for fluoride ion.

Langmuir isotherm criterion [52] can be described in term of dimensionless constant which is known as separation factor, R_L which can be defined as:

$$R_L = \frac{1}{1+K_L C_o} \qquad (3)$$

where C_o is the initial concentration of fluoride ion (mgL^{-1}). The feasibility of adsorption can be predicted from the values of R_L. For a favourable adsorption, the condition is: $0<R_L<1$. In

the present investigation, the values of R_L were found to be between 0 and 1 at all the temperatures studied which indicated the adsorption of fluoride onto CTet-HZO is a favourable process.

The linear form of the Freundlich equation is defined as: [53]

$$lnq_e = lnK_F + \frac{1}{n} lnC_e \qquad (4)$$

Where K_f represents the adsorption capacity constant and 1/n is related to the adsorption intensity. The values of K_f and n were calculated from the intercept and slope of the plot of log q_e against logC_e (Figure 9b) and summarized in Table 1. The values of K_f increased with increasing temperatures from 308 to 328 K, indicating that the adsorption processes were endothermic in nature. In general, the value of n> 1 indicates a favourable sorption process [54] and higher the n value stronger the adsorption intensity [55] In the present investigation, the values of n were found to be 1.48 1.65, and 1.93 at 308, 318 and 328 K, respectively, which indicated the adsorption of fluoride onto CTet-HZO is favourable. The increase of n value with the increase in temperature suggested increase in adsorption intensity and endothermic nature of the adsorption process. [56]

The application of Temkin isotherm [57] model is based on the assumptions: (i) adsorption process is characterized by uniform distribution of binding energies; (ii) a linear relationship exists between adsorbate-adsorbent interactions with a decrease of heat of adsorption for all the molecules covered in a layer. The linear form of Temkin equation is expressed as:

$$q_e = \beta\, lnA_T \; + \beta lnC_e \qquad (5)$$

$$\beta = \frac{RT}{b_T}$$

Where A_T is the equilibrium binding constant corresponding to the maximum binding energy (L/mg), b_T is Temkin isotherm constant related to heat of adsorption (J/mol). The values of A_T and b_T can be obtained from the intercept and slope of the plots of q_e Vs $\ln C_e$ (Figure 9c) and reported in Table 1.

The average percentage error (APE) analysis was used for comparison of all isotherm models using the following equation:

$$\mathrm{APE} = \frac{\sum_{i=1}^{n}(q_{e,exp} - q_{e,cal})/q_{e,exp}}{N} \times 100 \qquad (6)$$

Here, $q_{e,cal}$ and $q_{e,exp}$ represent the equilibrium capacity calculated from the isotherm models (mgg^{-1}), and equilibrium capacity from the experimental data. The values of APE of each model are presented in Table 1.

On the basis of coefficient of determination ($r^2 > 0.998$) and low values of APE, it can be suggested that experimental data fit well with Freundlich isotherm model followed by Temkin and Langmuir models. Similar observations on applicability of the experimental data to Freundlich model have been reported for adsorption of fluoride by alginate based anion exchanger, [58] Zr-Mn composite materials [59] and chitosan bead. [60]

3.3. Thermodynamic feasibility of the process

The thermodynamic Parameters such as change in free energy (ΔG°), enthalpy (ΔH°) and entropy (ΔS°) were calculated using the following equations;

$$\Delta G° = -RT\ln K_c \qquad (7)$$

$$\log K_c = \Delta S°/2.303R - \Delta H°/2.303RT \qquad (8)$$

where , $K_C = {}^{q_e}/_{C_e}$

K_c is the equilibrium constant, R the universal gas constant (8.314 J (mol K) $^{-1}$), and T the absolute temperature (K). The Vant's Hoff plot (logK_c against 1/T; Figure 10) gave a straight line and the values of $\Delta H°$ and $\Delta S°$ were evaluated from the slope and intercept. The values of $\Delta H°$ and $\Delta S°$ were found to be 4.98kJmol^{-1} and 18.43 J mol^{-1}K^{-1}, respectively. The values of $\Delta G°$ were -6.98, -8.82 and -10.66 KJmol^{-1} at 308, 318 and 328 K, respectively. The results illustrate that the fluoride adsorption on CTet-HZO surface is spontaneous and endothermic in nature.

3.4.Adsorption Kinetics:

Kinetic behaviour of CTet-HZO towards fluoride adsorption was studied as a function of time at a fixed initial concentration of fluoride ion (20 ppm) and at temperatures 308, 318 and 328 K. The time-dependent adsorption data were interpreted by pseudo-first order, pseudo-second-order and intraparticle diffusion models.

The linear form of pseudo-first order kinetic model [61] is expressed as:

$$\log(q_e - q_t) = log q_e - (\frac{k_1}{2.303})t \qquad (9)$$

Where k_1 is the rate constant of the pseudo-first-order adsorption process (min^{-1}),q_e and q_t are the amount of fluoride adsorbed at equilibrium and at time t (mg/g), respectively. A plot of log (q_e-q_t) against time yielded a straight line (Figure S8; SI) and the rate constant k_1 was evaluated from the slope (Table 3).

The linear form of pseudo second order kinetic model [62] is given by the following equation:

$$t/q_t = 1/k_2 q_e^2 + 1/q_e\, t \qquad (10)$$

where k_2 is the rate constant for the pseudo-second order adsorption reaction (gmg^{-1}min^{-1}). The value of k_2 and q_e were evaluated from the slope and intercept of the linear plot of t/qt versus t (Figure S8; SI) and results are reported in (Table 3).The applicability of a particular

kinetic model for CTet-HZO-fluoride system was examined on the basis of correlation coefficient values (R^2) and average percentage error (APE). As can be seen from the table that pseudo second order model with higher values of correlation coefficient and lower values of APE can accurately describe the experimental data.

3.4.1. Intraparticle Diffusion

The adsorption of an adsorbate onto an adsorbent can occur in three consecutive steps: (i). film diffusion, (ii) intra-particle diffusion, and (iii) adsorption on the interior surface of the adsorbent. The possible contribution of intraparticle diffusion on fluoride adsorption was investigated by a model given by Webber and Morris [63] which is expressed as:

$$q_t = k_{id} t^{0.5} + C_i \qquad (11)$$

where k_{id} is the intraparticle diffusion rate constant (mg $g^{-1}min^{0.5}$) and C_i is the intraparticle diffusion constant, which is directly proportional to the boundary layer thickness. According to Weber and Morris model, the plots of q_t versus $t^{0.5}$ should be linear if intraparticle diffusion is involved and if the lines pass through the origin, then the intraparticle diffusion is the rate controlling step. [63, 64] When the plots do not pass through the origin, then some degree of boundary layer control is suggested. If the data exhibit multi-linear plots, then two or more steps influence the sorption process. [49,63,64,65] Therefore, to decide on the main rate limiting step, q_t was plotted against $t^{0.5}$ for the sorption of fluoride on CTet-HZO (Figure 11). As can be seen from figure that the first region would describe the external resistance to mass transfer that is boundary layer diffusion. The second region is being dominated by intraparticle diffusion, where intraparticle diffusion is the rate-controlling step. In the last region, the intraparticle diffusion starts to go slow, owing to the decrease in the fluoride concentration in the aqueous phase, as well as decrease in the active sites available for adsorption. Similar observations were reported for fluoride adsorption by Mg-Al-LDHs

nanoflakes.[56] The values of k_{id}, C_i, and the correlation coefficients corresponding to the second region of the linear fitting of the kinetic data are listed in Table 3. The value of C_i and K_{id} increases with increase in concentration which reflects the boundary layer effect. The high value of R^2 indicated that the intra-particle diffusion played a significant role in the sorption of fluoride onto CTet-HZO hybrid material. Based on these results it might be concluded that the intra-particle diffusion was not the only rate controlling step in the sorption of fluoride onto the CTet-HZO hybrid material. Therefore the adsorption process may be consisting of both the surface adsorption and intraparticle diffusion.

3.5.Application:

Three groundwater samples (GW-1 ,GW-2 and GW-3) ,acidic effluent from metal finishing industry(AE) and river water sample (Ganga River) were collected from Aligarh (GW-1, GW-2 and AE), Agra (GW-3) and Kanpur districts of U.P., India respectively. The physico chemical analysis of water samples is given in (Table S1; SI). CTet-HZO was used to remove fluoride from the water samplesGW-1,GW-2 and river water) by batch method.The pH of water sample (50 mL) was adjusted to 3.5 using HNO_3before applying to CTet-HZO.. A predetermined amount of CTet-HZO. was added to each sample. After 40 min of equilibration, the samples were filtered and fluoride ion concentration was determined. The results are reported in Table 4. As can be seen from the table that the removal of fluoride in different water samples was above 90 % which proved that the CTet-HZO has a promising application for water treatment.

The fixed bed column adsorption experiments were conducted to evaluate the applicability of CTet-HZO and HZO in the removal of fluoride from synthetic water sample, groundwater (GW-3) and acidic effluent of metal finishing industry (AE).The basic composition of feeding solutions were shown in SI Table S2.Results (Figure12) indicated that the effective treatable volume of synthetic water sample, groundwater and acidic

effluent with CTet-HZO were around 160 mL, 180 mL and 320 mL, respectively, when the breakthrough point was set as 1.5 mg L^{-1}. The treatable volumes of synthetic water sample, groundwater and acidic effluent with HZO reached upto 105mL, 120 mL and 30 mL, respectively (Figure S9, SI).The Zr(IV) and diamine were not detected in the treated water. The results have suggested that CTet-HZO is more efficient than HZO in removing the fluoride from groundwater and acidic effluent of metal finishing industry.

3.6. Reuse and Regeneration of CTet-HZO

Regeneration and reuse of adsorbent materials is particularly required to reduce the cost factor. Desorption of fluoride from fluoride loaded CTet-HZO was carried out at varying concentrations of NaOH. It was observed that leaching of fluoride from the adsorbent material increased from 15.2 % to 98.67 % with increasing NaOH concentration from 0.02 to 0.1M. Further addition of increased NaOH concentration did not improve the leaching of F^- from the adsorbent. Hence, 0.1 M NaOH was used as a suitable desorbing agent. The adsorption of fluoride onto CTet-HZO followed by desorption with 0.1 M NaOH solution up to 10 cycles was studied. Results (Figure 13) show that adsorption (%) of fluoride on the regenerated materials was negligibly affected up to 4 cycles but percent adsorption gradually decreased from 98.67 % to 91.2 % with increasing regeneration cycles from 4 to 10. The study suggested that the material can be effectively used for removal of fluoride from aqueous system.

4. Conclusion:

In summary, we have prepared cyclic tetra [(indolyl)-tetra methyl]-diethane1,2-diamine (CTet) impregnated hydrous zirconium oxide. The synthesis was done in three steps.

- Firstly hydrous zirconium oxide gel was prepared.
- Secondly, cyclic tetramer of indole (CTet) was prepared by involving Mannich Base.
- Finally, CTet was incorporated into the hydrous zirconium oxide.

I. The fluoride adsorption capacity was found to be 188.68 mg/g. The enhanced capacity was mainly due to interaction between indole-NHs and fluoride ions.

II. The experimental adsorption data were analyzed by Langmuir, Freundlich and Temkin isotherm models. The coefficient of determination (R^2) and APE values indicated that Freundlich model describes the best fit of experimental data.

III. The adsorption of fluoride onto CTet-HZO follows the pseudo second order kinetic model.

IV. The thermodynamic parameters ($\Delta G° < 0$; $\Delta H° > 0$) suggest the sorption process is spontaneous & endothermic in nature. The remarkable advantage of this material is its chemical and mechanical stability due to the host organic molecule during successive sorption-desorption cycles.

V. CTet-HZO was found to be more effective than HZO for remediation of fluoride from drinking water.

• **Acknowledgments:**

The authors are thankful to UGC (DRS-II) and DST (FIST and PURSE) for facilities to carry out this work. Uzma Haseen and Mohammad Fazeel Khan are grateful to UGC for providing financial support to complete the research work. We are also thankful to USIF, A.M.U. Aligarh for SEM and TEM; SAIF, Punjab University, Chandigarh for XRD.

†Electronic Supplementary Information (ESI) available: [details of any supplementary information is available free of charge via the Internet. www.rsc.org/suppdata/esi.

References:

[1] I. Pauling, *The nature of chemical bond,* 3rd Edn; Cornell university press Ithaca, New York: 1960.

[2] J. Fawell, K. Bailey, J. Chilton, E. Dahi, L. Fewtrell and Y. Magara*, Fluoride in drinking water, World Health Organisation,* published by IWA Publishing, London, UK, **2006,** p-5.

[3] R. Tekle-Haimanot, Z. Melaku, H. Kloos, S. Reimann, W. Fantye, L. Zerihun and K. Bajorvatn, *Sci. Total. Environ.,* 2006, **367,** 182-190.

[4] M. Amini, K. Mueller, K.C. Abbaspour, T. Rosenberg, M. Afyuni, K.N. Moller, M. Sarr and C.A. Johnson, *Environ. Sci. Technol.,* 2008, **42,** 3662-3668.

[5] WHO, *Fluoride and oral health. Report of a WHO expert committee on oral health status and fluoride use,* WHO Technical Report Series, No. 846; Geneva, 1994 http://whqlibdoe.who.int/trs/WHO_TRS_846.pdf.

[6] P.E. Petersen and M.A. Lennon, *Community Dent. Oral Epidemiol.,* 2004, **32,** 319-322.

[7] *United State Environmental Pollution Agency (USEPA), National primary drinking water standards,* EPA/ 816-F/03/016, 2003.

[8] WHO. *Guidelines for drinking water quality,* 3rd Edn. World health Organisation, Geneva, Switzerland, 2004.

[9] C. Gonzales, H. Hotokezaka, E. I. Karadeniz, T. Miyazaki, E. Kobayashi, M. A. Darendeliler and N. Yoshida, *Am. J. Ortho Dentofacial Orthop.* 2004, **139,** 196-205.

[10] I.B. Solangi, S. Memon and M.I. Bhanger, *J. Hazard. Mater.*, 2009, **171,** 815-819.

[11] Rajiv Gandhi National Drinking Water Mission (RGNDWM), *Prevention and control of fluorosis in India.* 1993.

[12] S.S. Tripathi, J. Bersillon and K. Gopal, *Sep. Purif. Technol.,* 2006, **50,** 310-317.

[13] M.F. Chang and J.C. Liu, *J. Environ. Eng.,* 2007, **133,** 419-425.

[14] L.A.B.S. Richards, H.M.A. Rossiter and A.I. Schafer, *Desalination,* 2009, **248,** 177-183.

[15] S. Chakrobortty, M. Roy and P. Pal, *Desalination,* 2013, **313,** 115-124.

[16] A.N. Ghanim, *Int. J. Environ. Sci.,* 2014, **4,** 660-675.

[17] M. Arda, E. Orhan, O. Arar, M. Yusksel and N. Kabay, *Sep. Sci. Technol.,* 2009, **44,** 841-853.

[18] Bhatnagar, E. Kumar and M. Sillanpaa, *Chem. Eng. J.,* 2011, **171,** 811-840.

[19] J. Qiao, Z. Cui, Y. Sun, Q. Hu and X. Guan, *Environ. Sci. Eng.*, 2014, **8,** 169-179.

[20] M. Mohapatra, D. Hariprasad, L. Mohapatra, S. Anand and B.K. Mishra, *Appl. Surf. Sci.,* 2012, **258,** 4228-4236.

[21] T. Wajima, Y. Umeta, S. Narita and K. Sugawara, *Desalination,* 2009, **249,** 323-330.

[22] S.K. Swain, T. Patnaik and R.K. Dey, *Desalination Water. Treat.,* 2013, **51,** 4368-4378.

[23] A.L. Srivastava, P.K. Singh, V. Srivastava and Y. C. Sharma, *J. Hazard. Mater.,* 2013, **263,** 342-352.

[24] M.R. Boldaji, A.H. Mahvi, S. Dobaradaran and S.S. Hosseini, *Int. J. Environ. Sci. Technol.,* 2009, **6,** 629-632.

[25] R. K. Dey, S.K. Swain and T. Patnaik, *ARPN J. Sci. Technol.,* 2012, **2,** 138-142.

[26] Q. Zhang, Q. Du, T. Jiao, Z. Zhang, S. Wang, Q. Sun and F. Gao, *Sci. Rep.,* 3:2551, **2013,** DOI: 10.1038/srep02551, 1-9.

[27] M. D. Santi, L. Galluzi, S. Lucarini, M.F. Poletti, A. Fraternale, A. Duranti, C.D. Marco, M. Fanilli, N. Zaffaroni, G. Brandi and M. Magnani, *Breast Cancer Res. Treat.,* 2011, **13,** 1-15.

[28] M. D. Santi, A. Antonelli, M. Menotta, C. Sfara, S. Sarafini, S. Lucarini, G. Brandi and M. Magnani, *J. Nanopharmaceutics Drug Delivery,* 2013, **1,** 45-51.

[29] M. K Suk, N.-K. Chae, U.-I. Kim, J.-M. Kim and K.-S. Jeong, *Pure Appl. Chem.,* 2008, **80,** 599–608.

[30] B. Deka and R. J. Sarma, *Sens. Actuators A,* 2014, **197,** 321-325.

[31] R.R. Gupta, M. Kumar and V. Gupta, *Heterocyclic chemistry Vol. II* Springer international Edition. Springer (India) Pvt. Limit. New Delhi, 2005; pp 226-228.

[32] K. Biswas, D. Bandhoyapadhay and U.C. Ghosh, *Adsorption,* 2007, **13,** 83-94.

[33] X. Dou , D. Mohan, U. Charles Pittman, Jr. And S.Yang, *Chem. Eng. J. (Amsterdam, Neth.),* 2012, **199,** 236-245.

[34] K. Nakamoto, *Infrared and Raman spectra of Inorganic and Co-ordination compounds, Part B*, 6th Edn; John Wiley & sons inc. Publication, 2009, pp 16-17.

[35] G. Socrates, *Infrared Characteristics Group Frequencies,* 3rd Edn; John Wiley & Sons: New York, 1980.

[36] J.T.R. Dunsmuir and A.P. Lane, *Spectrochim. Acta, Part A,* 1972, **28,** 45-50.

[37] H.F.Castro, M.L.C.P.Silva and G.L.J.P.Silva, Brazilian J.Chem.Eng., 2000, **17** , 849-857.

[38] C.Hang, Q.Li, S.Gao and J.K.Shang, Ind.Eng.Chem.Res., 2012, **51**, 353-361.

[39] Y. Tang, J. Wang and N. Gao, *J. Environ. Sci.,* 2010, **22,** 1689–1694.

[40] B. Pan, J.U. B. Wu, Z. Li and X. Liu, *Environ. Sci. Technol.,* 2013, **47,** 9347-9354.

[41] N. Rahman and U. Haseen, *Ind. Eng. Chem. Res.,* 2014, **53,** 8198−8207.

[42] Langmuir, *J. Am. Chem. Soc.,* 1918, **40,** 1361−1403.

[43] Y-H. Lia, S. Wang, X. Zhanga, J. Weia, C. Xua, Z. Luanb and D. Wua, *Mater. Res. Bull.,* 2003, **38,** 469–476.

[44] A.T. Sequeira, M. S. Rios, V.M. Miranda and I. L. Hernandez, *J. Coll. Interface Sci.,* 2014, **418,** 254–260.

[45] J. Wang, W. Xu, L. Chen, Y. Jia, L. Wang, X-J. Huang and J. Liu, *Chem. Eng. J.,* 2013, **231,** 198–205.

[46] Y-H. Li, S. Wang, A. Cao, D. Zhao, X. Zhang , C. Xu, Z. Luan, D. Ruan, J. Liang, D. Wu and B. Wei, *Chem. Phys. Lett.,* 2001, **350,** 412–416.

[47] M. S. Onyango, Y. Kojima, O. Aoyi, E.C. Bernardo and H. Matsuda, *J. Coll. Interface Sci.,* 2004, **279,** 341–350.

[48] M. Mohapatra, T. Padhi, S. Anand and B.K Mishra, *Desalin. Water Treat.,* 2012, **50,** 376-386.

[49] M.G. Sujana, A. Mishra and B.C. Acharya, *Appl. Surf. Sci.,* 2013, **270,** 767-776.

[50] G. Chakrabarti, S. K. Biswas and U.C. Ghosh, *Appl. Surf. Sci.,* 2014, **307,** 665–676.

[51] Y. Li, P. Zhang, Q. Du, X. Peng, T. Liu, Z. Wang, Y. Xia, W. Zhang, K. Wang, H. Zhu and D. Wu, *J. Coll. Interfaces Sci.,* 2011, **363,** 348-354.

[52] K. R. Hall, L. C. Eagletow, A. Acrivers and T. Vermenlem, *Ind. Eng. Chem. Fund.,* 1966, **5,** 212-223.

[53] H.M.F. Freundlich, *J. Phys. Chem.,* 1906, **57,** 385-470.

[54] G. Jayapriyal, R. Ramya1, X. R. Rathinam and P.N. Sudha, *Arch. Appl. Sci. Res.,* 2011, **3,** 415-423.

[55] J.U.K. Oubagaranadin, N. Sathyamurthy and Z.V.P. Murthy, *J. Hazard. Mater.,* 2007, **142,**165-174.

[56] C. Gao, X-Y. Yu, T. Luo, Y. B. Jia, J. Sun, H. Liu and X. J. Huang, *J. Mater. Chem. A.,* 2014, **2,** 2119-2128.

[57] R.D. Johnson and F.H. Arnold, *Biochim. Biophys. Acta.,* 1995, **1247,** 293-297.

[58] H. Paudyal, B. Pangeni, K. Inou, H. Kawakita, K. Ohto, K.N. Ghimire and S. Alam, *Biores. Technol.,* 2013, **148,** 221-227.

[59] V. Tomar, S. Prasad and D. Kumar, *Microchem. J.,* 2013, **111,** 116-124.

[60] N. Viswanathan, C.S. Sundaram and S. Meenakshi, *J. Hazard. Mater.,* 2009, **161,** 423-430.

[61] S. Lagergren, *Kungl. Sven. Ventenskapsakad. Handl.,* 1898, **24,** 1-39.

[62] Y.S. Ho and G. Mckay, *Can. J. Chem. Eng.,* 1998, **76**, 822-827.

[63] J. W. J. Weber and J. C. Morris, *J. San. Eng. Div. Proceed. Am. Soc. Civ. Eng.,* 1963, **89,** 31-60.

[64] N. Chen, Z. Zhang, C. Fang, N. Sugiura, M. Li and R. Chen, *J. Coll. Interface Sci.,* 2010, **348,** 579-584.

[65] M. J. Yu, F. Zhou, L. Jin, L. Yang, M. Luan, J. Tang, Y. Fan, H. Yuan and Z. J. Chen, *ACS Appl. Mater. Interfaces,* 2012, **4**, 5749-5760.

Figure Caption:

Scheme 1. Preparation of cyclic tetra [(indolyl)-tetra methyl]-diethane 1,2-diamine (CTet).

Scheme 2. Functionalization of HZO with cyclic tetra [(indolyl)-tetra methyl]-diethane 1, 2-diamine (CTet) at optimal reaction condition.

Scheme 3. Sorption mechanism of fluoride onto CTet-HZO.

Figure 1. FT-IR spectra: (a) hydrous zirconium oxide, (b) modified hydrous zirconium oxide (CTet-HZO).

Figure 2. X-ray diffraction pattern (a) CTet-HZO (b) fluoride sorbed CTet-HZO.

Figure 3. SEM images: (a) hydrous zirconium oxide (b) CTet-HZO and (c) Fluoride sorbed CTet-HZO.

Figure 4. TEM image of CTet-HZO

Figure 5. ^{13}C NMR spectrum of CTet-HZO.

Figure 6. TGA and DTA curves (a) HZO and (b) CTet-HZO material.

Figure 7. Effect of pH variation. Concentration; 20 mgL^{-1}; contact time; 40 min; adsorbent dose; 0.15g)

Figure 8. Bar diagram showing the percentage uptake of fluoride ion in presence of interfering ions.

Figure 9. Equilibrium adsorption isotherms of F^- onto CTet-HZO (a) Langmuir model (b) Freundlich model (c) Temkin model.

Figure 10. Van't Hoff plot for adsorption of fluoride onto CTet-HZO.

Figure11. Plot of q_t versus $t^{0.5}$ for the sorption of fluoride ion onto CTet-HZO at different temperatures.

Figure 12. Removal of fluoride from different feeding solution by column method using CTet-HZO as sorbent (a) synthetic water sample, fluoride concentration = 5.0 mg L^{-1}; pH 6.8 (b) groundwater (GW-3), fluoride concentration = 3.6 mg L^{-1}; pH 6.8 (c) acidic effluent (AE), fluoride concentration = 4.20 mg L^{-1}; pH 4.1.

Figure 13. Bar diagram showing the percentage uptake of fluoride by CTet-HZO in different cycles of batch operation.

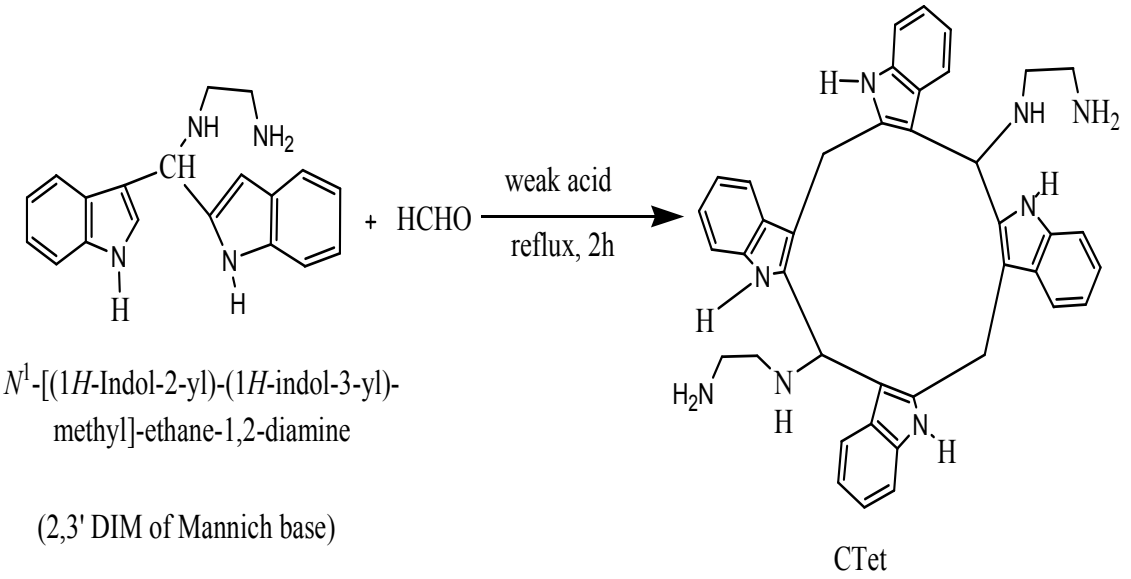

N^1-[(1*H*-Indol-2-yl)-(1*H*-indol-3-yl)-methyl]-ethane-1,2-diamine

(2,3' DIM of Mannich base)

CTet

Scheme 1: Preparation of cyclic tetra [(indolyl)-tetra methyl]-diethane 1,2-diamine (CTet).

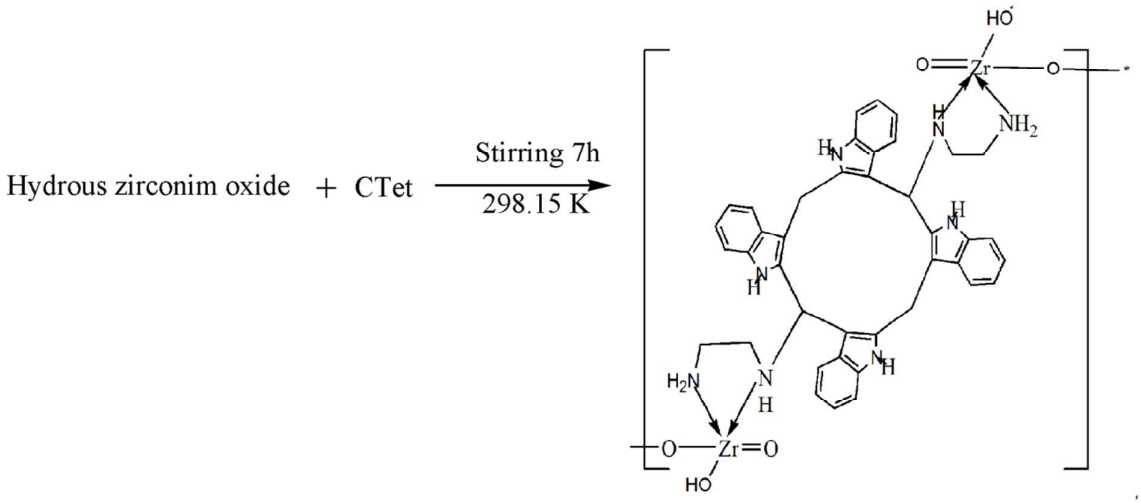

(CTet-HZO)

Scheme 2: Functionalization of HZO with cyclic tetra [(indolyl)-tetra methyl]-diethane 1,2-diamine (CTet) at optimal reaction condition.

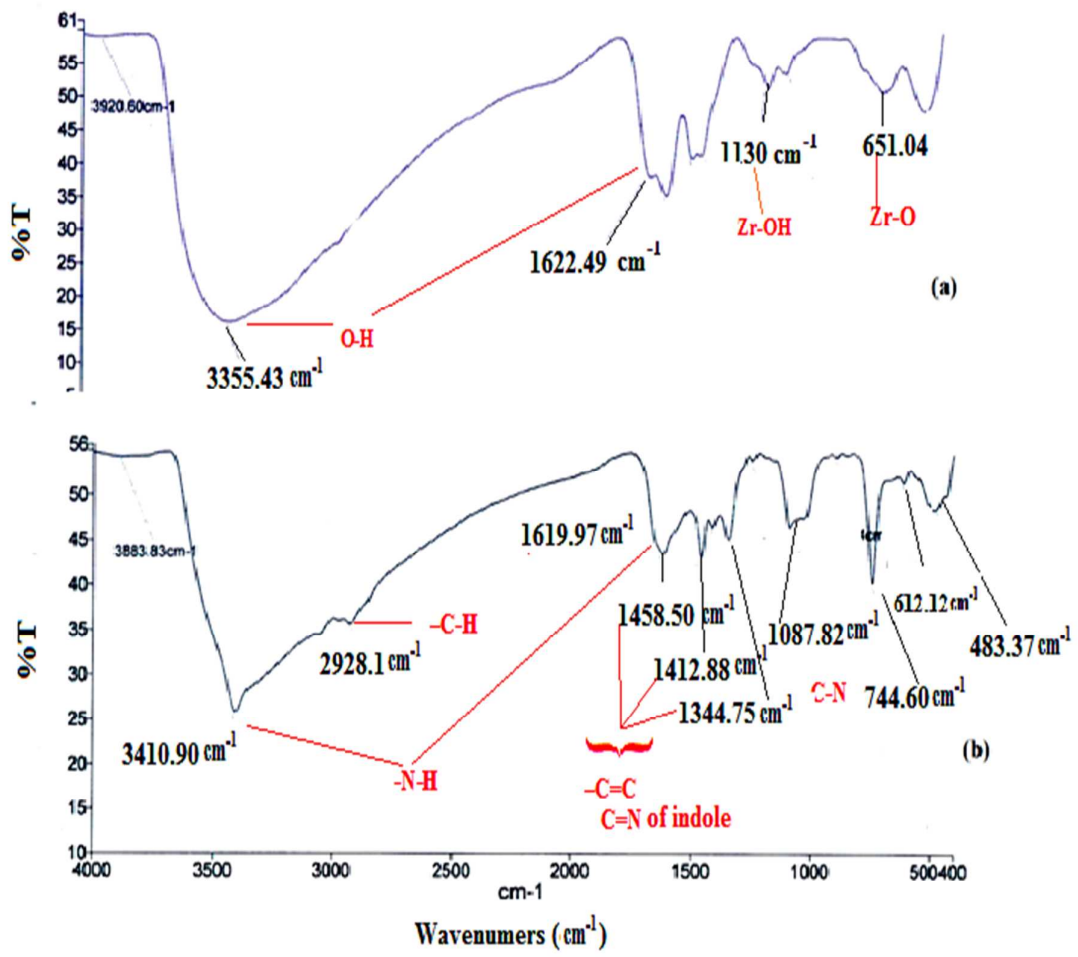

Figure 1. FT-IR spectra of (a) hydrous zirconium oxide (b), and modified hydrous zirconium oxide (CTet-HZO).

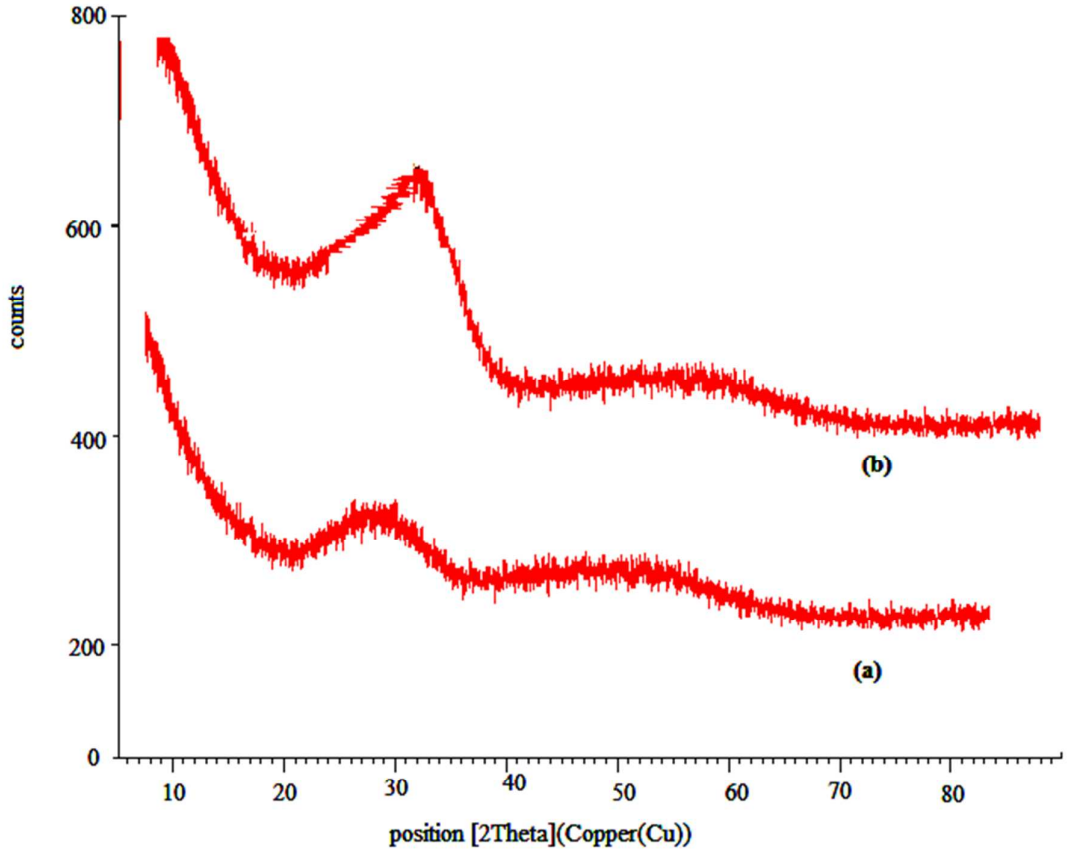

Figure 2. X-ray diffraction pattern of (a) CTet-HZO (b) fluoride sorbed CTet-HZO.

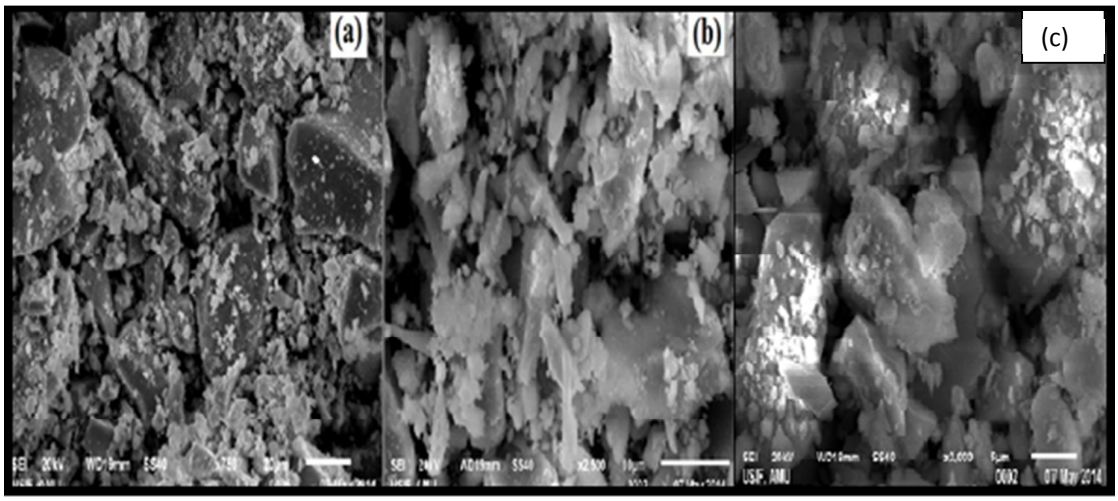

Figure 3. SEM images (a) hydrous zirconium oxide (HZO) (b) CTet-HZO and (c) Fluoride sorbed CTet-HZO.

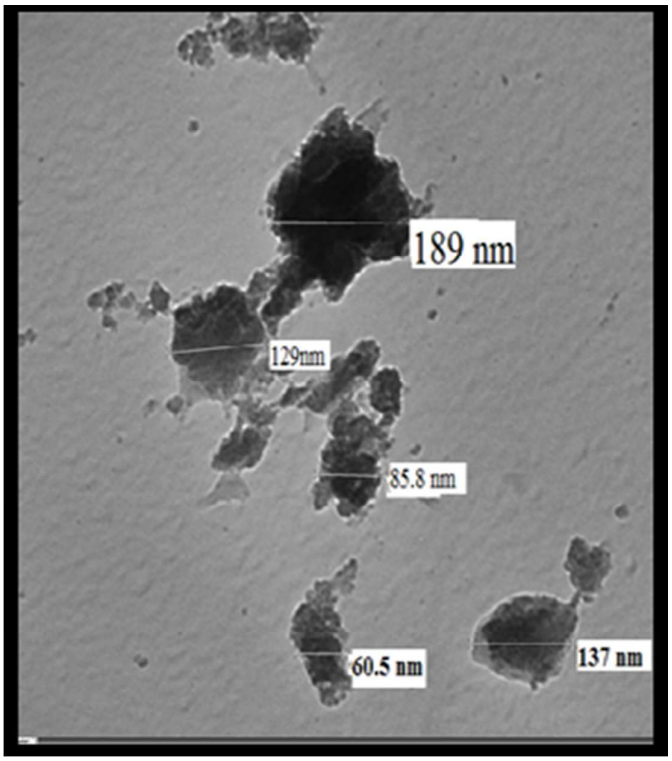

Figure 4. TEM image of CTet-HZO

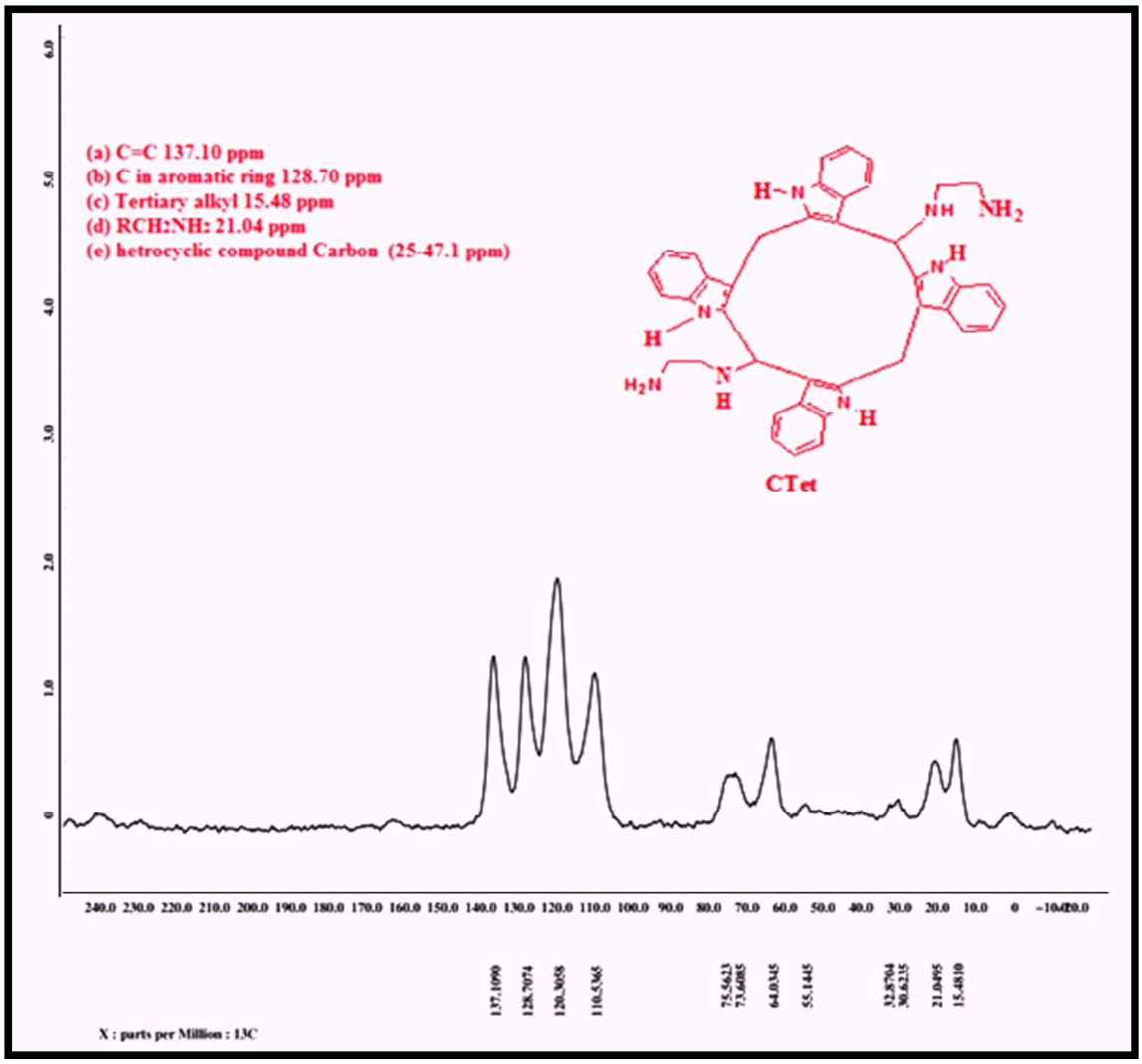

Figure 5. ^{13}C NMR spectrum of CTet-HZO.

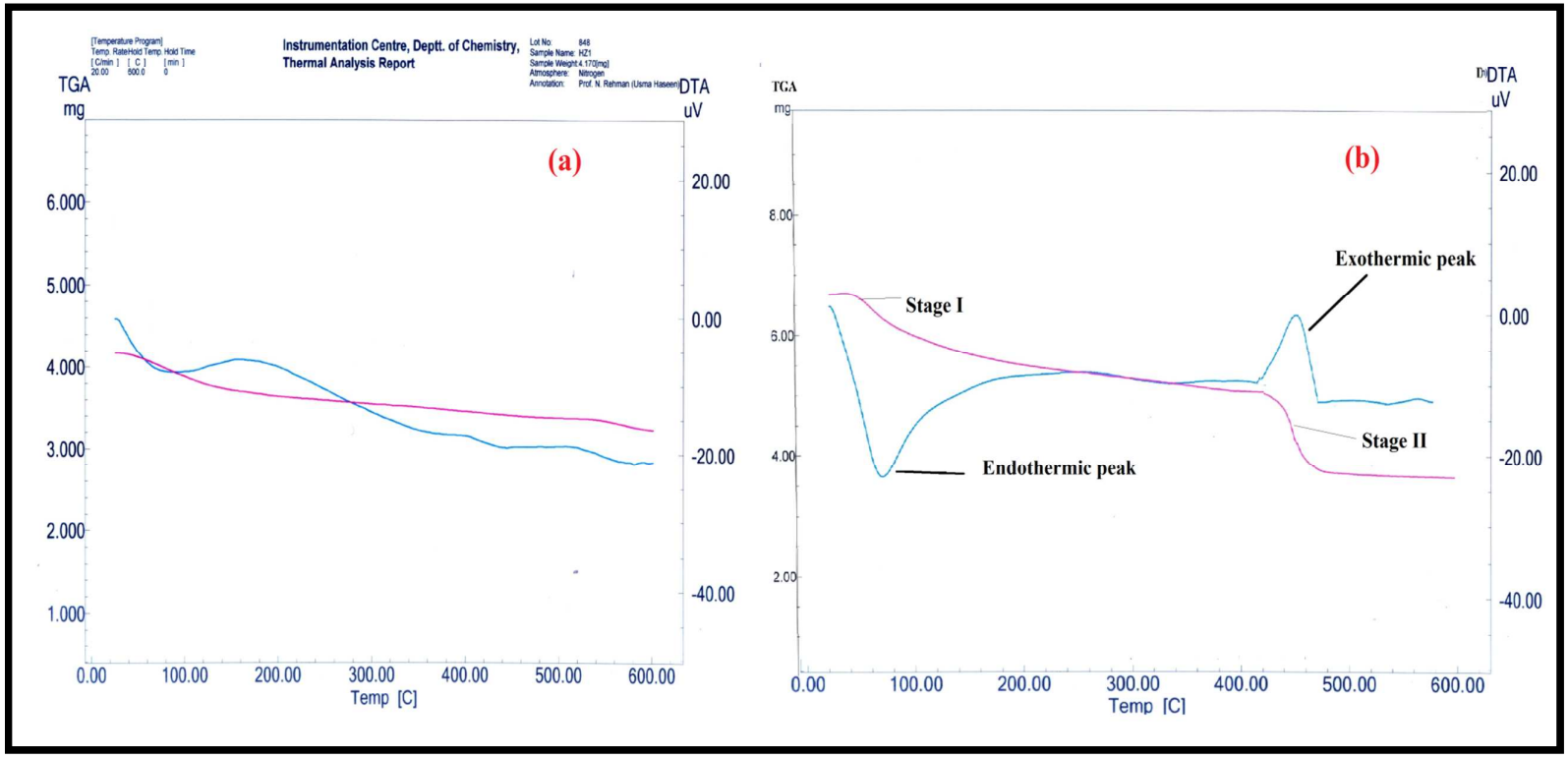

Figure 6. TGA and DTA curves :(a) HZO (hydrous zirconium oxide), (b) CTet-HZO material.

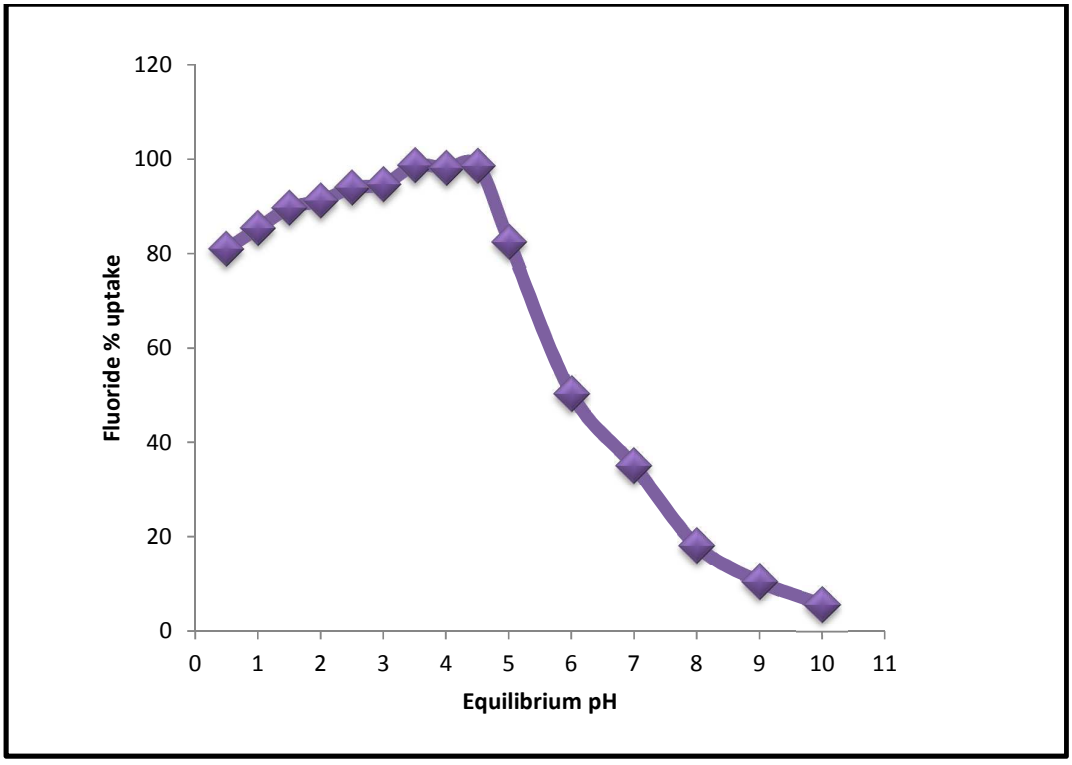

Figure 7. Effect of pH variation. Concentration; 20 mgL^{-1}; contact time; 40 min; adsorbent dose; 0.15g)

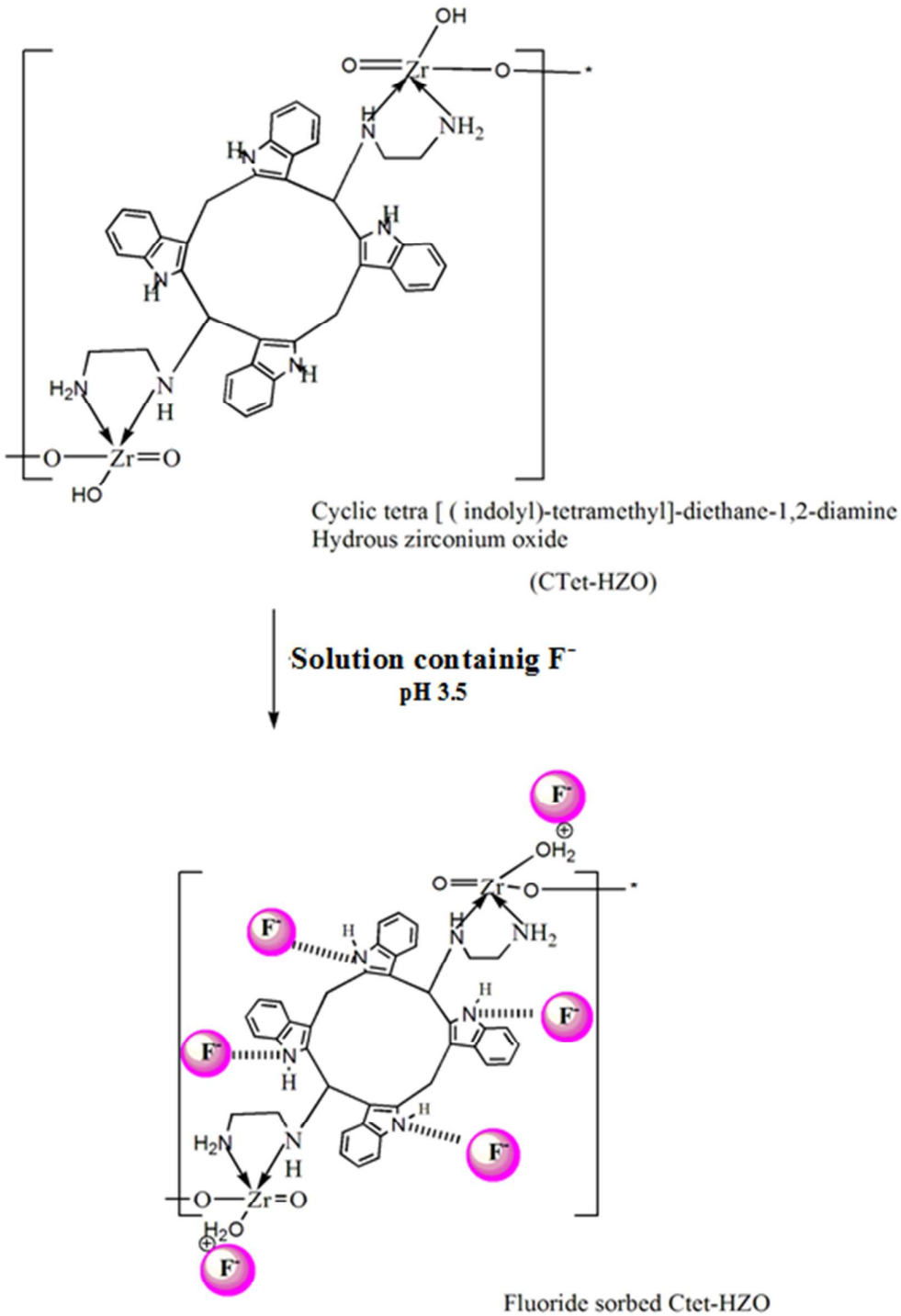

Scheme 3: Sorption mechanism of fluoride onto CTet-HZO.

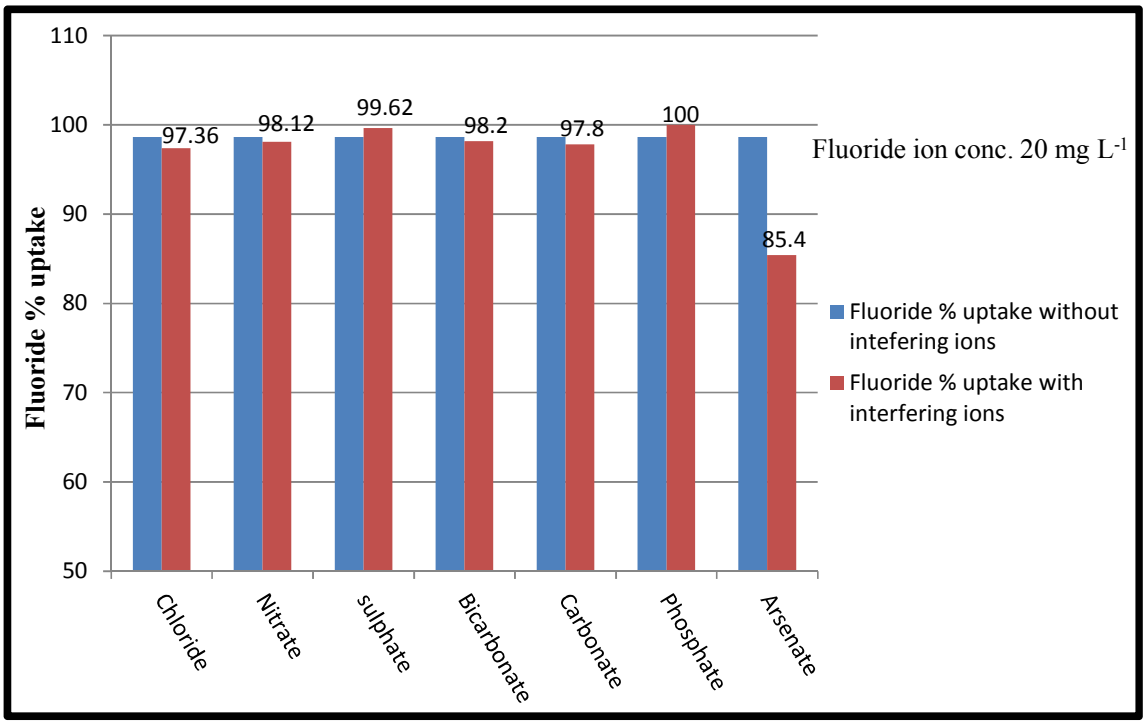

Figure 8. Bar diagram showing the percentage uptake of fluoride ion in presence of interfering ions.

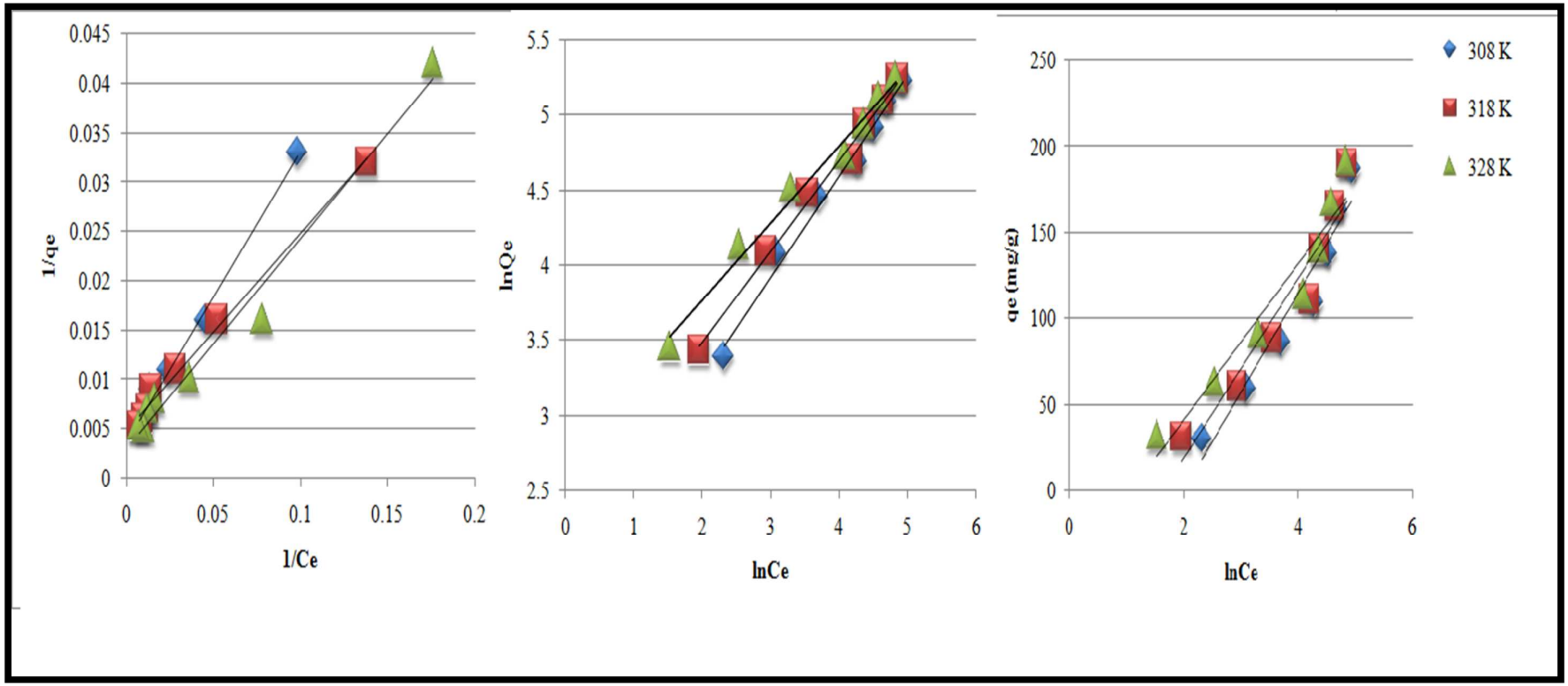

(a) (b) (c)

Figure 9. Equilibrium adsorption isotherms of F^- onto CTet-HZO (a) Langmuir model (b) Freundlich model (c) Temkin model.

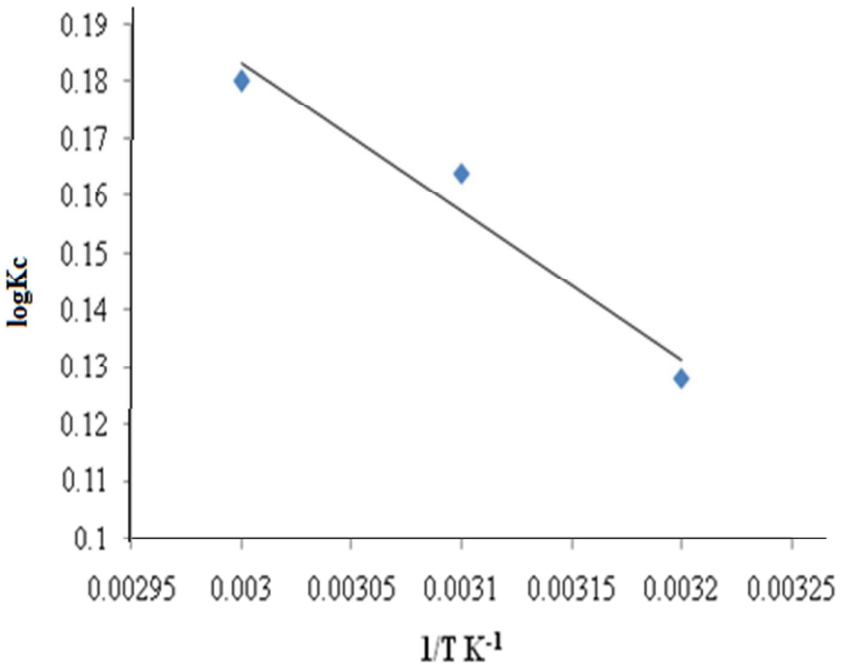

Figure 10. Van't Hoff plot for adsorption of fluoride onto CTet-HZO.

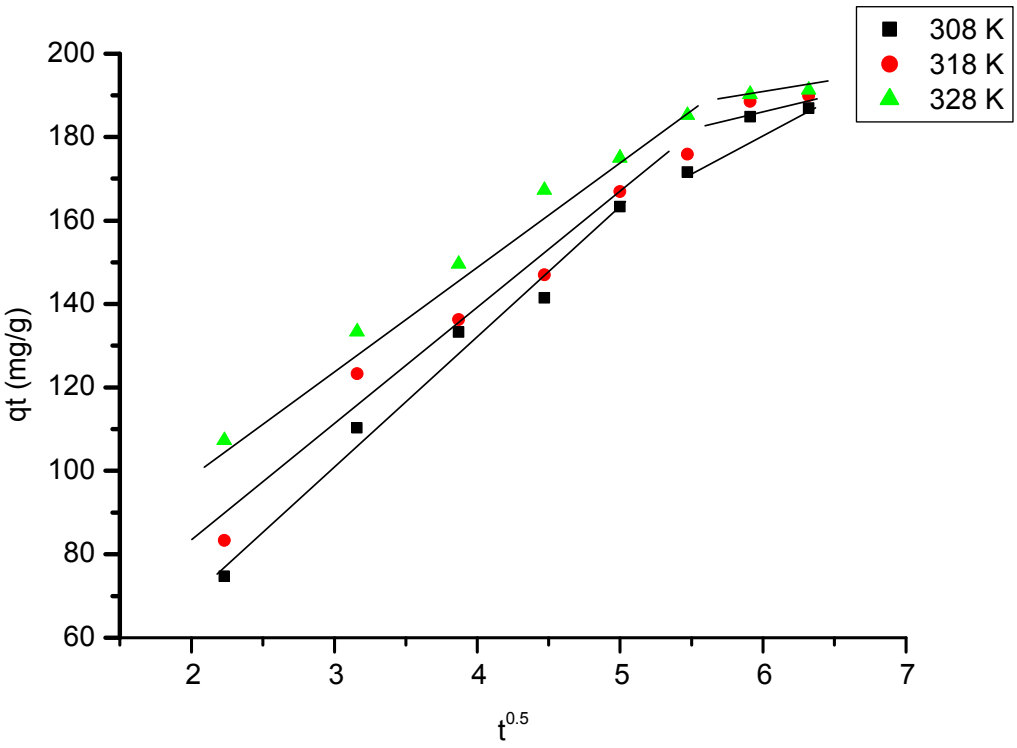

Figure11. Plot of q_t versus $t^{0.5}$ for the sorption of fluoride ion onto CTet-HZO at different temperatures.

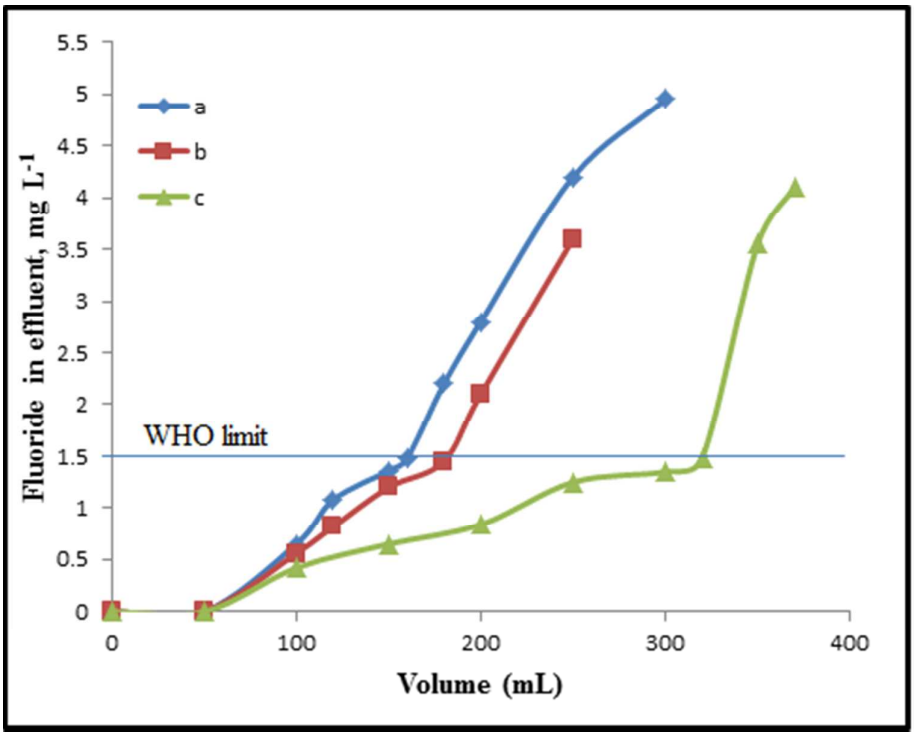

Figure 12. Removal of fluoride from different feeding solution by column method using CTet-HZO as sorbent (a) synthetic water sample, fluoride concentration = 5.0 mg L^{-1}; pH 6.8 (b) groundwater (GW-3), fluoride concentration = 3.6 mg L^{-1}; pH 6.8 (c) acidic effluent (AE), fluoride concentration = 4.20 mg L^{-1}; pH 4.1.

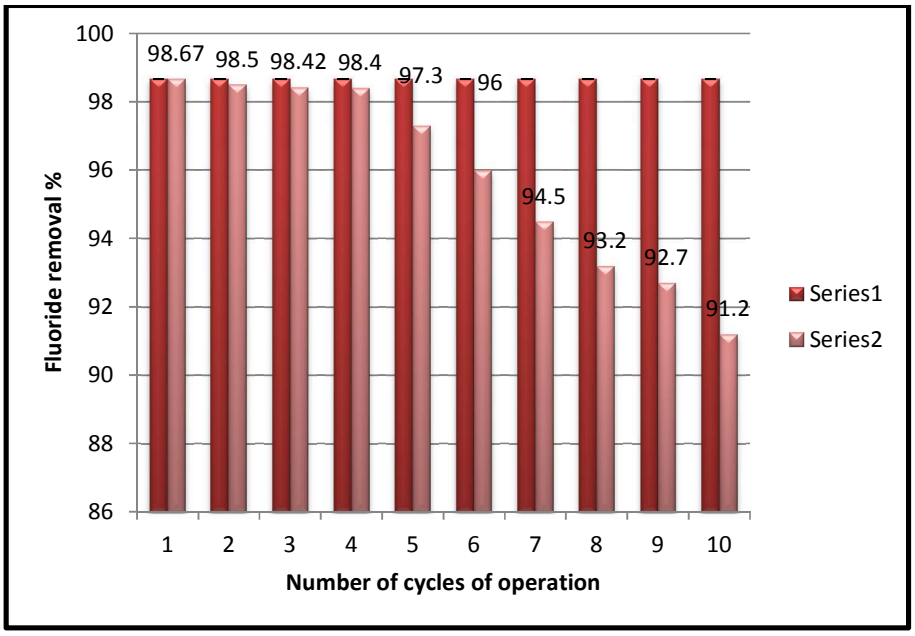

Figure 13. Bar diagram showing the percentage uptake of fluoride by CTet-HZO in different cycles of batch operation.

Table Caption:

Table 1: Isotherm parameters of Langmuir, Freundlich and Temkin models for the adsorption of fluoride onto CTet-HZO at different temperatures

Table 2: Comparison of fluoride adsorption capacities and equilibrium time of different adsorbents reported in the literature with present study.

Table 3: Adsorption kinetic parameters of different models.

Table 4: Removal of fluoride ion from samples collected from different sources by CTet- HZO.

Table 1. Isotherm parameters of Langmuir, Freundlich and Temkin models for the adsorption of fluoride onto CTet-HZO at different temperatures.

Isotherm	**Temperature (K)**	**Parameters**				**Error Function**
		q_m (mgg^{-1})		K_L	R^2	APE
Langmuir	308	333.33		0.010	0.993	11.18
	318	204.08		0.020	0.991	4.5
	328	196.07		0.021	0.980	2.31
		q_m (mgg^{-1})	K_f	n	R^2	APE
Freundlich	308	185.4	6.69	1.48	0.988	0.463
	318	183.48	9.66	1.65	0.991	0.486
	328	188.68	15.31	1.93	0.995	0.11
		q_m (mgg^{-1})	b_T	A_T	R^2	APE
Temkin	308	167.73	44.46	0.133	0.939	1.46
	318	168.21	49.40	0.191	0.925	1.63
	328	169.60	60.07	0.335	0.930	1.61

Table 2: Comparison of fluoride adsorption capacities and equilibrium time of different adsorbents reported in the literature with present study.

Sorbents	Equilibrium time	Fluoride adsorption capacity (mgg^{-1})	pH	Reference
Aligned carbon nanotubes	1 h	3.0	7.0	[43]
Aluminium modified hematite	24 h	10.3	6.2	[44]
CeO_2–ZrO_2 nanocages	24 h	175	4.0	[45]
Al_2O_3/CNTs	-	14.9	6.0	[46]
Al^{3+}-exchanged zeolite	24h	37.5	6.5	[47]
CTAB mediated Mg-doped nano Fe_2O_3	4h	49.2	7.0	[48]
Hydrous ferric oxide doped alginate beads	1.5 h	8.9	7.0	[49]
Hydrous Ce(IV)–Zr(IV) mixed oxide	1.5 h	19.5	5.8	[50]
Graphene	110 min	48.3	3.6-10.2	[51]
Hydrous zirconium oxide	45 min	124, 68	4.0,7.0	[33]
Hydrous zirconium oxide (HZO)	90 min	54.6	6-7	This study
CTet-HZO	40 min	188.6	3.5-4.5	This study

Table 3: Adsorption kinetic parameters of different models.

Temp K	**Pseudo-first –order or Lagergren model**					**Pseudo-second-order model**			**Intra particle diffusion model**		
	$q_{e,exp}$	k_1	$q_{e,cal}$	R^2	APE	k_2	$q_{e,cal}$	APE	K_{id}	C	R^2
308	4.35	0.257	18.1	0.913	105	0.0627	4.69	2.6	0.021	0.193	0.883
318	4.85	0.310	25.0	0.867	138.4	0.0453	4.85	0	0.104	0.499	0.909
328	4.93	0.274	11.3	0.917	43.06	0.0379	5.05	0.81	0.148	2.055	0.921

Table 4: Removal of fluoride ion from water samples collected from different sources using CTet- HZO by batch method

Sample No.	Permissible limit (mgL^{-1})	Initial Fluoride ion concentration (μgmL^{-1})	Fluoride ion concentration after adsorption (μgmL^{-1})	RSD (%)	Removal (%)
GW-1	1.5/WHO*	1.84	0.067	5.90	96.46
GW-2	1.5/WHO -	3.62	0.056	1.79	98.45
RW	1.5/WHO -	2.68	0.142	1.69	94.70

*WHO= World Health Organization
RW= river water